

# Hyaluronic acid stimulates neovascularization during the regeneration of bone marrow after ablation

Andrew L. Raines,<sup>1,2</sup> MoonHae Sunwoo,<sup>3</sup> Arthur A. Gertzman,<sup>3</sup> Kipling Thacker,<sup>4</sup> Robert E. Guldberg,<sup>1,5</sup> Zvi Schwartz,<sup>1,2</sup> Barbara D. Boyan<sup>1,2</sup>

<sup>1</sup>Parker H. Petit Institute for Bioengineering and Bioscience, Georgia Institute of Technology, Atlanta, Georgia

<sup>2</sup>Wallace H. Coulter Department of Biomedical Engineering at Georgia Tech and Emory University, Georgia Institute of Technology, Atlanta, Georgia

<sup>3</sup>Musculoskeletal Transplant Foundation, Edison, New Jersey

<sup>4</sup>Lifecore Biomedical LLC, Chaska, Minnesota

<sup>5</sup>Woodruff School of Mechanical Engineering, Georgia Institute of Technology, Atlanta, Georgia

Received 13 April 2010; revised 5 October 2010; accepted 18 November 2010

Published online 10 January 2011 in Wiley Online Library (wileyonlinelibrary.com). DOI: 10.1002/jbm.a.33012

**Abstract:** Restoration of vasculature is a critical component for successful integration of implants in musculoskeletal tissue. Sodium hyaluronate (NaHY) has been used as a carrier for demineralized bone matrix (DBM). DBM is osteoinductive and osteoconductive, but whether NaHY by itself has an effect is not known. NaHY has been reported to promote neovascularization, suggesting it may increase neovasculature when used with DBM as well. To test this, we used a rat tibial marrow ablation model to assess neovascularization during bone formation and regeneration of marrow with different combinations of NaHY alone and NaHY+DBM. To assess neovascularization during normal healing, animals were euthanized at 3-, 6-, 14-, 21-, and 28-days post-ablation, and the vasculature perfused using a radio-opaque contrast agent. Vascular morphology was assessed using  $\mu$ CT and histology. Peak vessel volume within the marrow cavity was observed on day-14 post-ablation. Test materials were injected into the

ablated marrow space as follows: (A) empty defect controls; (B) high MW (700–800 kDa) NaHY + heat inactivated DBM; (C) DBM in PBS; (D) low MW NaHY (35 kDa) + DBM; (E) high MW NaHY + DBM; (F) D:E 50:50; (G) low MW NaHY; (H) high MW NaHY; and (I) G:H 50:50. Neovascularization varied with bone substitute formulation.  $\mu$ CT results revealed that addition of NaHY resulted in an increase in vessel number compared to empty defects. Total blood vessel volume in all NaHY only groups were similar to DBM alone. Histomorphometry of sagittal sections showed that all three formulations of NaHY increased blood vessel number within the marrow cavity, confirming that NaHY promotes neovascularization. © 2011 Wiley Periodicals, Inc. *J Biomed Mater Res Part A*: 96A: 575–583, 2011.

**Key Words:** rat tibial bone marrow ablation, vasculogenesis, microCT using a contrast agent to label vasculature, histomorphometry, DBM plus hyaluronic acid

## INTRODUCTION

A common objective when using biomedical implants, particularly in musculoskeletal tissues, is rapid apposition of host tissue to the implant surface. Currently, several regenerative medicine therapies exist for the restoration and augmentation of bone in orthopaedic and dental applications, including autologous and allogeneic bone grafts as well as synthetic bone graft substitutes. While autologous bone is still the “gold standard” within the field because of its biocompatibility as well as its source of stem cells and growth factors,<sup>1,2</sup> allografts and synthetic bone substitutes also provide an osteoconductive surface to promote bone growth. A critical requirement for the survival of any bone graft is the rapid ingrowth of blood vessels from the surrounding tissue.<sup>3</sup>

Hyaluronic acid is a high molecular weight ( $10^4$ – $10^7$  Da), negatively charged, non-sulfated glycosaminoglycan consisting of repeating units of *N*-acetylglucosamine and *D*-glucuronic acid.<sup>4</sup> It is a component of the extracellular matrix (ECM) expressed in nearly all tissue types<sup>4</sup> and plays

an important role in tissue morphogenesis and healing.<sup>5,6</sup> During wound healing, native hyaluronic acid serves as an anti-angiogenic molecule, inhibiting endothelial cell proliferation and migration.<sup>7</sup> These observations have led to the use of the sodium salt of hyaluronic acid (NaHY) in a number of wound healing applications.<sup>8</sup> Although NaHY inhibits capillary formation in a three dimensional collagen gel,<sup>7,9</sup> low molecular weight degradation products of NaHY have been demonstrated to stimulate vascular endothelial cell proliferation,<sup>10–14</sup> migration,<sup>15</sup> collagen synthesis,<sup>16</sup> sprout formation,<sup>17</sup> and new blood vessel formation.<sup>18</sup>

Allogeneic bone graft substitutes like demineralized bone matrix (DBM) are used as filler materials to enhance the healing of fractures and to help regenerate bone in osseous defects.<sup>19</sup> Because the particulate, powdery nature of DBM results in poor handling qualities, it is often combined with materials to improve its handling characteristics for surgical procedures.<sup>19,20</sup> Commonly used materials for this process include NaHY, calcium sulfate, glycerol, and gelatin.<sup>19</sup> The

**Correspondence to:** B. D. Boyan; e-mail: barbara.boyan@bme.gatech.edu

combination of DBM with these materials creates a more gelatinous substance, allowing for easier insertion and molding into osseous defect sites. DBM is known to promote bone formation by virtue of its osteoinductive and osteoconductive properties, but whether NaHY can also stimulate bone formation when used as a cofactor with DBM is not known. NaHY has also been reported to accelerate bone healing.<sup>21</sup> The exact mechanism by which NaHY promotes bone healing is unknown, but one possibility is that it increases neovascularization in the newly forming bone. NaHY has already been shown to promote neovascularization in non-bony sites<sup>22</sup> and is being investigated for use as a scaffold material for angiogenic tissue engineering,<sup>23</sup> supporting this hypothesis.

The purpose of the present study was to determine if NaHY stimulates neovascularization during bone formation induced by DBM. The study took advantage of the rapid endosteal bone formation that occurs following injury to the marrow cavity of rat tibial bone.<sup>24</sup> The rat bone marrow ablation model is an established model for examining bone formation and remodeling.<sup>25</sup> It has been well characterized in a number of academic laboratories and it is used by industry to assess osteogenic properties of biomaterials as well as pharmaceuticals.<sup>26,27</sup> The model is also applicable for assessing endosteal bone formation and remodeling in orthopaedics following placement of intramedullary rods and joint prostheses.<sup>28</sup> In this model, the bone marrows of rat tibias are flushed of cells. A blood clot and granulation tissue fill the marrow space over the first three days of healing. Primary bone begins to form on the endosteal surface by day 6 and eventually fills the marrow cavity. Remodeling of the newly formed bone occurs between days 12 and 25, resulting in resorption of the primary bone. By day-35 post-ablation, replacement of the primary bone with bone marrow is complete, resulting in the regeneration of normal tissue phenotype.<sup>29</sup> This process follows a well-documented time table,<sup>25,30</sup> which makes it a very useful model for the study of normal bone repair and for the evaluation of extrinsic and intrinsic factors that may influence it. The enclosed environment of the marrow space restricts the distribution of test materials and localizes their effects, thus allowing the model to be useful for the study of the effects of biomaterials that have been designed for bone augmentation.

In this study, neovascularization occurring within the ablated marrow cavity was assessed over time by perfusing the vasculature of rats with a radio-opaque silicone contrast agent and imaging the vasculature using micro-computed tomography ( $\mu$ CT). To determine the role of NaHY in stimulating neovascularization during endosteal bone formation, we placed various formulations of NaHY with and without DBM in the ablated marrow space of rats. Vascular morphology of the ablated limbs was assessed 14 days post-ablation using both  $\mu$ CT analysis as well as histology.

## MATERIALS AND METHODS

### Materials

Implant materials were prepared by the Musculoskeletal Transplant Foundation (MTF, Edison, NJ) and packaged in

sterile syringes. Materials were able to be extruded through an 18-gauge needle, which is the largest size able to fit into the hole created for the marrow ablation. The DBM used for the study was from a single donor and was shown to be osteoinductive in the mouse gastrocnemius muscle pouch assay. DBM particulates ranged in size from 212 to 500  $\mu$ m in diameter.

### Marrow ablation

The Institutional Animal Care and Use Committee (IACUC) at the Georgia Institute of Technology approved all animal procedures. Eight-week-old male immunocompromised (rNu/rNu) rats were purchased from Harlan Laboratories (Harlan, Indianapolis, IN). Rats were anesthetized with isoflurane gas inhalation, laid on their backs and covered with a sterile surgical drape. The surgical area was shaved and disinfected with providone iodine. An incision was made over the diaphysis of the tibia and the surrounding muscles were moved aside using blunt dissection to expose the bone. A round perforation was made in the mid-diaphysis through the cortical bone using a 0.9-mm round dental bur. Marrow was excavated with an inverted cone dental bur and the marrow space was then flushed with sterile, physiological saline.

A time course study was first performed to determine the time at which neovascularization was greatest. The marrow space was left empty, and the covering muscles were returned to their normal positions and the skin incision was closed with wound clips. Immediately after recovery from anesthesia, rats were injected with buprenorphine to relieve pain. Animals had access to food and water *ad libitum* for the duration of the study. At days 3, 6, 14, 21, and 28 post-ablation, animals ( $n = 3$ ) were perfused-fixed and imaged as described below. Based on the results of the time course study, 14-days post-ablation was selected as the endpoint for the DBM + NaHY study.

To examine the role of NaHY in promoting neovascularization during endosteal bone formation, we ablated the marrow of rat tibias and injected test compounds ( $v \sim 125 \mu$ L) corresponding to the groups outlined in Table I. The left hind tibias of  $n = 9$  animals were ablated for each group.

### Vascular perfusion

Following anesthetization, the abdominal cavity of rats was opened and the internal organs were moved aside. A 22-gauge 1" catheter was inserted into the descending aorta and the caudal vena cava was severed to allow for the vasculature to be flushed. About 250  $\mu$ L of heparin (1000 U  $\text{mL}^{-1}$ ) was injected into the catheter to prevent clotting of the blood. The vasculature was flushed with 0.9% normal saline using a peristaltic pump set to a flow rate of 15  $\text{mL min}^{-1}$ . Specimens were subsequently pressure fixed with 10% neutral buffered formalin. Formalin was flushed from the vessels with 0.9% normal saline, and the vasculature was injected with a radio-opaque silicone rubber compound containing lead chromate (Microfil MV-122, Flow Tech, Carver, MA), according to the manufacturer's protocol. Animals were stored at 4°C overnight to allow for contrast agent polymerization. Rat hind

**TABLE I. Materials Injected into the Medullary Canal Following Marrow Ablation**

Group No.	Carrier	DBM	Comments
A	No carrier	No DBM	Empty defect
B	Carrier I: 3.8–4.0% solution of 700–800 kD NaHY in PBS buffer pH 7.4	31%	Heat denatured DBM; negative control for test system
C	0.9% Saline	31%	No NaHY carrier, DBM baseline
D	Carrier I: 3.8–4.0% solution of 700–800 kD NaHY in PBS buffer pH 7.4	31%	Represents commercial DBX <sup>®</sup> putty
E	Carrier II: 3.8–4.0% solution of 35 kD NaHY in PBS buffer pH 7.4	31%	Low MW NaHY carrier with 31% DBM
F	Carrier I 50:50 Carrier II mixture	31%	Equal mixture of the two carriers with 31% DBM
G	Carrier I: 3.8–4.0% solution of 700–800 kD NaHY in PBS buffer pH 7.4	0%	Carrier for commercial DBX putty, no DBM
H	Carrier II: 3.8–4.0% solution of 35 kD NaHY in PBS buffer pH 7.4	0%	Low MW NaHY carrier only, no DBM
I	Carrier I 50:50 Carrier II mixture	0%	50:50 mixture of the two carriers only, no DBM

A total of  $n = 9$  animals were used per each treatment group.

limbs were dissected from the specimens and soaked for 4 days in 10% neutral buffered formalin to ensure complete tissue fixation prior to  $\mu$ CT imaging.

#### $\mu$ CT image analysis

Tissue samples were imaged using a high-resolution desktop micro-CT imaging system (vivaCT; Scanco Medical,

Bassersdorf, Switzerland) as described by Duvall et al.<sup>31</sup> Briefly, samples were imaged using a 36- $\mu$ m voxel size with a voltage of 55 kV and a current of 109  $\mu$ A. Serial image sections were created in a 1024  $\times$  1024 pixel image matrix. Serial tomograms were reconstructed from raw data using a cone beam filtered back-projection algorithm.<sup>32</sup> Noise was reduced using a low pass Gaussian filter ( $\sigma = 1.2$ ,

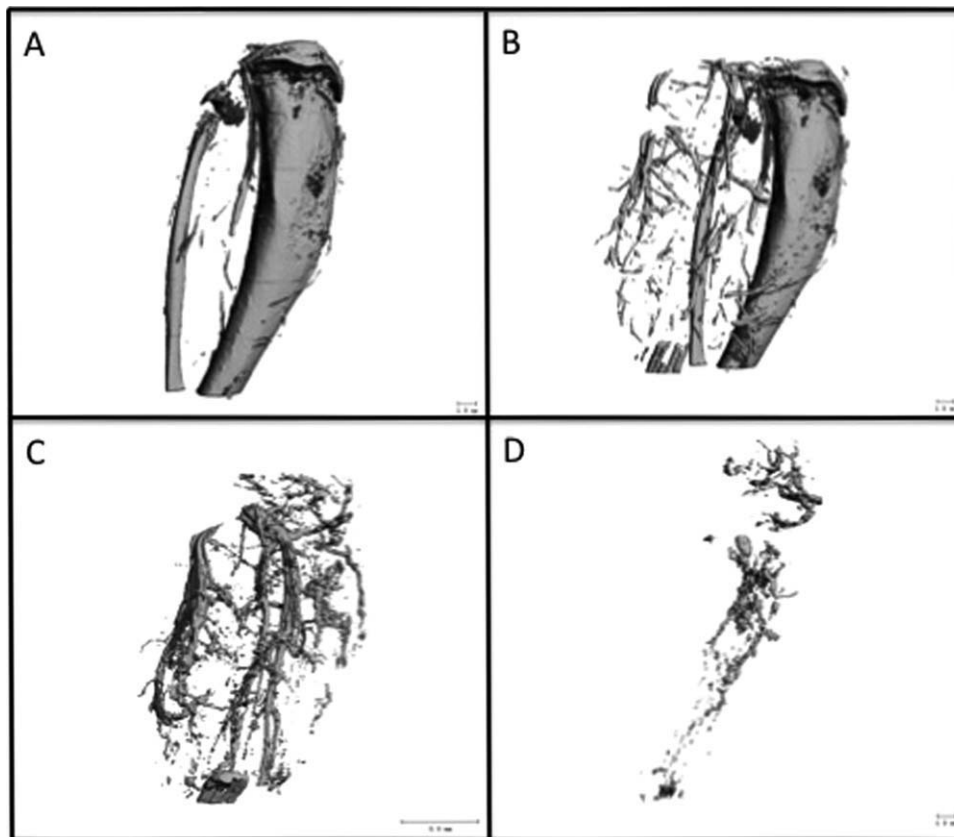


**FIGURE 1.** To demonstrate feasibility of the procedure, at the time of harvest, rat vasculature was perfused-fixed using 10% formalin and a radio-opaque silicone-based contrast agent (Microfil, Carver, MA). Ablated, perfused tibiae were imaged using  $\mu$ CT to examine the bone (A) and surrounding vasculature (B). Tissues were subsequently decalcified and imaged with  $\mu$ CT a second time to isolate the vasculature both surrounding (C) and within (D) the ablated tibiae.

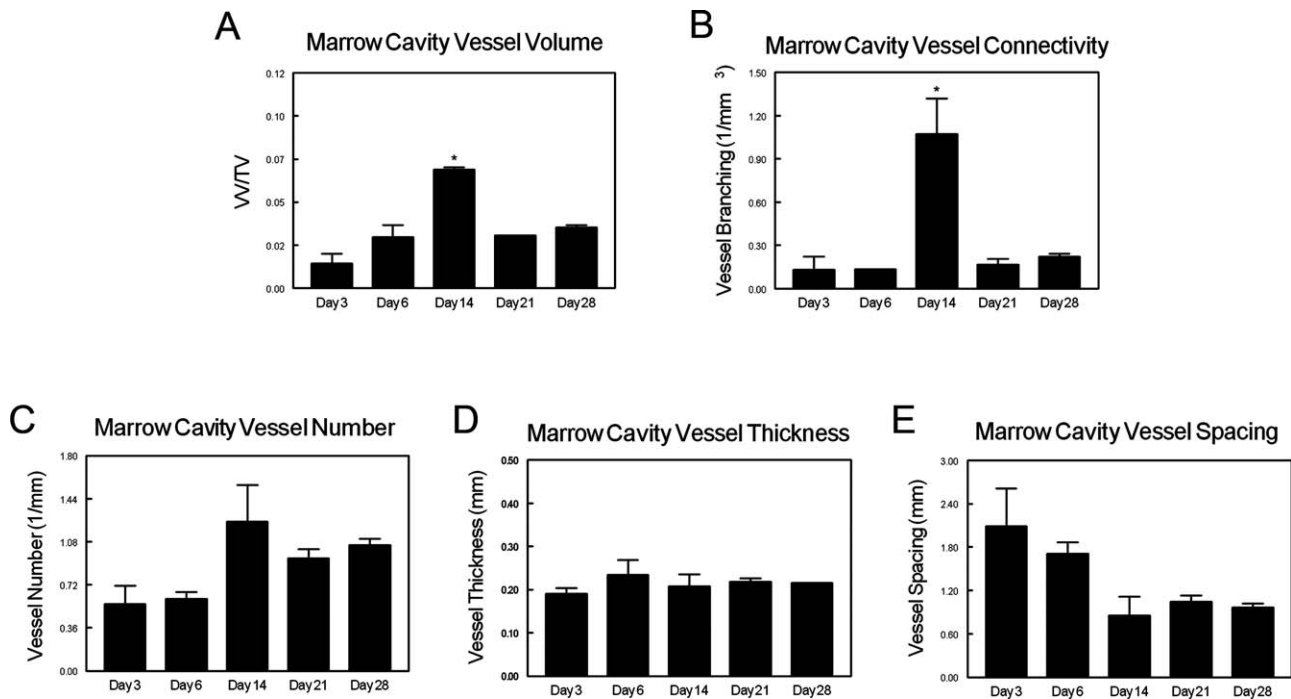


**FIGURE 2.** Time course of neo-vascularization following tibial marrow ablation. At days 3, 6, 14, 21, and 28 post-ablation, rats were perfused-fixed with Microfil (Flow-Tech, Carver, MA) and imaged using  $\mu$ CT. (A) Marrow cavity vessel volume fraction, (B) vessel connectivity, (C) vessel number, (D) vessel thickness, and (E) vessel spacing were quantitatively assessed. Data are presented as the mean  $\pm$  SEM of three animals for each time point. \* $p < 0.05$  versus all other time points.

support = 2). The serial tomograms were globally thresholded based on X-ray attenuation and used to render binarized three dimensional (3D) volume images of the repair gap vascular network. The parameters for three dimensional vascular morphology (vessel volume, number, connectivity, thickness, and spacing) were determined using the method described in detail by Duvall et al.<sup>31</sup> and were quantified with histomorphometric analysis based on direct distance transform methods.<sup>33,34</sup>

### Histology

Following decalcification and  $\mu$ CT imaging, samples were embedded in paraffin, and sectioned along the sagittal plane. The 5- $\mu$ m sections were stained with haematoxylin and eosin (H&E) to assess vascular structures. The number of blood vessels within the ablated marrow space was counted in four serial sections from each sample and the values were averaged to obtain the mean blood vessel number for each treatment group.

### Statistical analysis

Both  $\mu$ CT and histology data from each group were analyzed by ANOVA and when statistical differences were detected, Student's *t* test for multiple comparisons using Bonferroni's modification was used. *p* values  $< 0.05$  were considered statistically significant.

### RESULTS

Ablated, perfused tibias were imaged using  $\mu$ CT to examine the bone [Fig. 1(A)] and surrounding vasculature [Fig. 1(B)].

Samples were subsequently incubated for 72 h at 22°C in formic acid (CalEx II, Fisher Scientific, Pittsburgh, PA) to decalcify the bone and facilitate image segmentation of the vasculature both surrounding [Fig. 1(C)] and within [Fig. 1(D)] the ablated tibias. The region of interest (ROI) in 2D serial sections for vascular morphology analysis was determined by using the 2D sections of calcified images as a template for the selection of the appropriate area for the ablated marrow space. Assessment of the 3D vascular morphology for both the time course study and the NaHY + DBM study was done using the results based on the images like the one shown in Figure 1(D).

Neovascularization within the marrow cavity varied as a function of time post-ablation. Peak blood vessel volume within the marrow cavity was observed on day 14 [Fig. 2(A)] and was significantly higher at this time than at all other time points examined ( $p < 0.05$ ). Similarly, blood vessel connectivity also reached its maximum at day 14 [Fig. 2(B)].  $\mu$ CT analyses of blood vessel number [Fig. 2(C)], vessel thickness [Fig. 2(D)], and vessel spacing [Fig. 2(E)] did not reveal any significant differences amongst any of the time points examined. However, it should be noted that on day 14 post-ablation, a moderate increase in blood vessel number and a corresponding decrease in blood vessel spacing was observed. The average diameter of blood vessels in the marrow remained constant at all time points. Based on these data, it was determined that at 14-days post-ablation, neovascularization occurring within the ablated marrow cavity is at its peak and this time point was selected as the endpoint for the NaHY + DBM study.

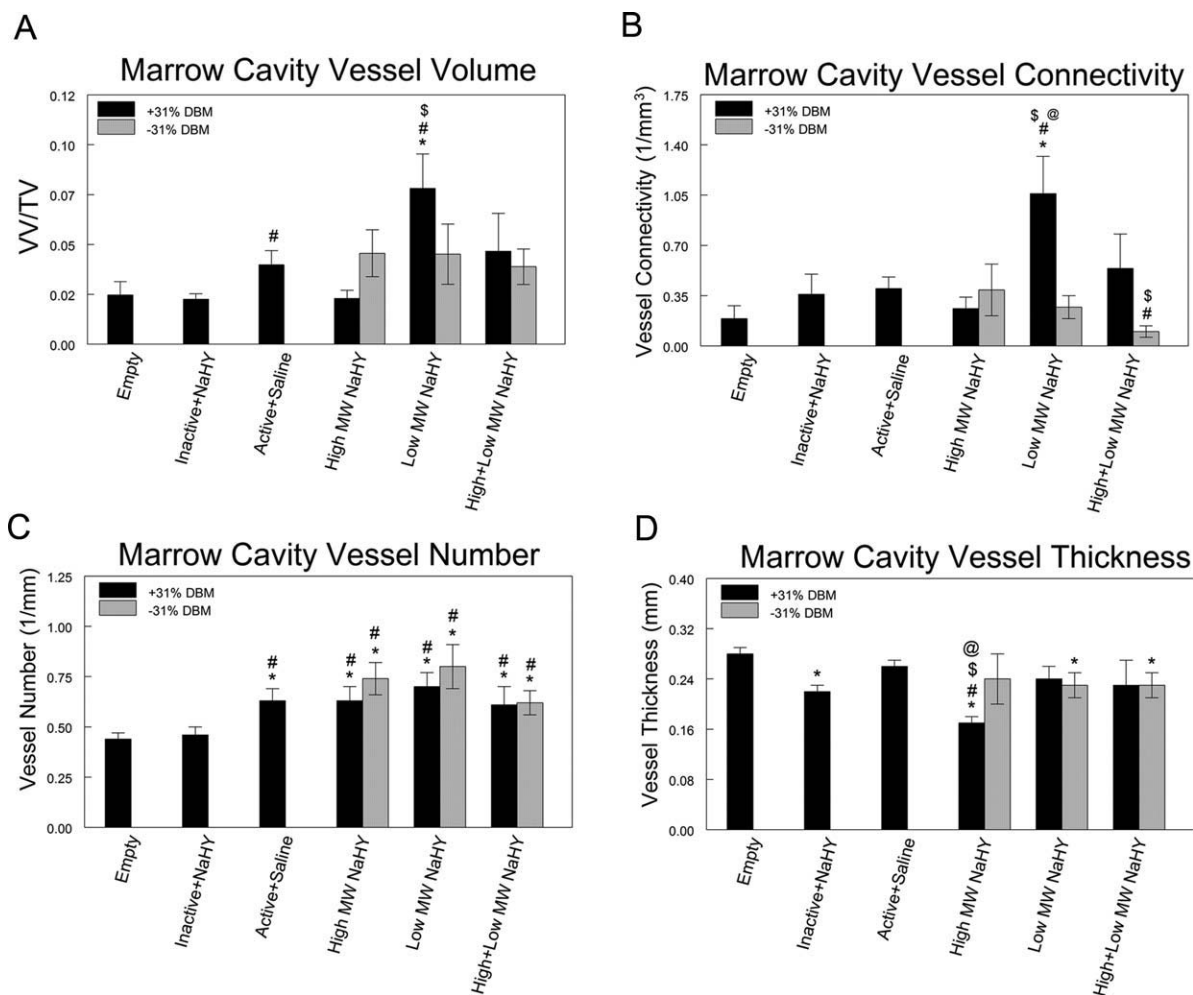


**FIGURE 3.** Influence of DBM and NaHY on neo-vascularization after tibial marrow ablation. At 14 days after marrow ablation and injection of test compounds, rats were perfused-fixed with Microfil and imaged with  $\mu$ CT. (A) Marrow cavity vessel volume fraction, (B) vessel connectivity, (C) vessel number, and (D) average vessel diameter (vessel thickness). Data are presented as the mean  $\pm$  SEM of nine animals per group. \* $p < 0.05$  versus empty defect; # $p < 0.05$  versus inactive + NaHY; \$ $p < 0.05$  versus active + saline; @ $p < 0.05$  versus no DBM.

$\mu$ CT analysis showed that neovascularization within the marrow cavity at 14-days post-ablation was sensitive to the formulations of NaHY and NaHY + DBM that were injected into the marrow space. DBM alone increased the total blood vessel volume fraction in the ablated marrow space compared to heat inactivated DBM ( $p < 0.05$ ) and empty defects (not significant). Addition of low MW NaHY to DBM further enhanced blood vessel volume within ablated marrows compared to empty defects, heat inactivated DBM and DBM alone. High MW NaHY, low MW NaHY, and high + low MW NaHY by themselves displayed moderate increases in total vessel volume compared to empty defects, although none of these were significant [Fig. 3(A)]. Similar to total blood vessel volume, the combination of low MW NaHY with DBM increased blood vessel connectivity compared to empty defects, DBM alone and NaHY alone. High and low MW NaHY decreased blood vessel connectivity compared to DBM alone [Fig. 3(B)].

Three dimensional  $\mu$ CT analysis of vessel number showed that all three formulations of NaHY administered either alone

or in combination with DBM as well as DBM alone increased the total number of blood vessels in ablated marrows compared to empty defects and heat inactivated DBM [Fig. 3(C)]. The average vessel diameter in the ablated marrow space was found to decrease in low MW NaHY and high + low MW NaHY groups compared to empty defects. High MW NaHY + DBM showed the lowest average vessel diameter amongst all treatment groups [Fig. 3(D)].

When combined with DBM, NaHY also increased the total volume fraction of radio-opaque tissue within the marrow cavity as observed by  $\mu$ CT. 31% DBM by itself did not have a larger bone volume fraction compared to empty defects, however the addition of low MW NaHY to 31% DBM significantly increased the volume of radio-opaque tissue within the marrow space compared to DBM alone. In addition, both high MW NaHY and low MW NaHY promoted new bone formation to a similar extent as DBM alone. The combination of high + low MW NaHY significantly reduced the formation of new bone compared to empty defects and DBM alone (Fig. 4).

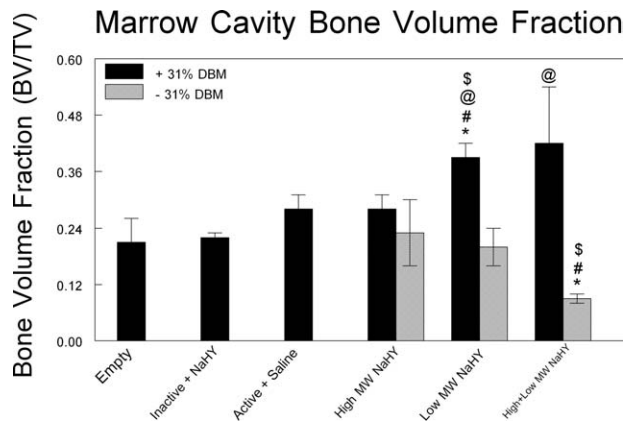


**FIGURE 4.** Marrow cavity new bone volume.  $\mu$ CT was used to assess the volume of new bone within marrow cavities 14 days after ablation. \* $p < 0.05$  versus empty; # $p < 0.05$  versus inactive + NaHY; \$ $p < 0.05$  versus active + saline; @ $p < 0.05$  versus no DBM.

To account for the volume occupied by the DBM within the ablated marrow cavities on reducing the volume available for neovascularization, we corrected the total blood vessel volume fraction in all experimental groups containing DBM. On the basis of observations from  $\mu$ CT scans, we estimated that DBM occupied  $\sim 60\%$  of the ablated marrow space. Figure 4 shows the total blood vessel volume fraction adjusted to subtract the volume occupied by DBM. The results demonstrate that in both the low MW NaHY + DBM and the high + low MW NaHY + DBM groups that when the volume occupied by DBM in the ablated marrows is removed, the blood vessel volume fraction is significantly increased compared to the treatment groups containing either low MW NaHY or high + low MW NaHY alone, respectively (Fig. 5).

Haematoxylin and eosin stained sagittal sections of the treated tibias showed the presence of new bone. Blood vessel structures containing Microfil were visible in cuts from all treatment groups (Fig. 6). Histomorphometric analysis of total marrow cavity blood vessel number showed that addition of low MW NaHY significantly increased the number of blood vessels compared to empty defects, heat inactivated DBM, active DBM, and a combination of low MW NaHY + 31% DBM (Fig. 7). Addition of both high MW NaHY and a combination of high + low MW NaHY increased the number of blood vessels in the marrow cavity compared to heat inactivated DBM.

## DISCUSSION

Successful bone formation surrounding implants is dependent on the establishment of a patent vasculature at the bone-implant interface. This study demonstrates that NaHY increases the number of new blood vessels in the ablated marrow cavity and suggests that it is also helps to promote osteogenesis. Both high and low MW NaHY increased the total vessel number compared to empty defects, with a corresponding decrease in average vessel diameter. Determination of the number of vascular structures of mid-sagittal sections supported the  $\mu$ CT observations. Overall, addition of

low MW NaHY to DBM resulted in an increase in the total vessel volume fraction and vessel connectivity within ablated marrows. In addition, a combination of low MW NaHY + DBM resulted in an increase in bone volume fraction compared to empty defects, DBM alone, and NaHY alone. This suggests that low MW NaHY may enhance osteogenesis when combined with DBM via increased vascularity as confirmed by greater numbers of smaller vessels.

Bone is a highly vascularized tissue, and the link between bone formation and vascular invasion is well established.<sup>35</sup> Vascularization of cartilage is a prerequisite for bone formation during growth and development<sup>36</sup> and the development of a vascular bed is necessary during fracture healing and bone repair and regeneration to allow for the migration of osteoprogenitor cells to the healing site as well as to supply oxygen and nutrients and allow for removal of waste.<sup>37</sup>

DBM is a commonly used bone graft substitute, because of its osteoconductive and osteoinductive properties. However, VEGF expression and micro-vessel density (MVD) are low during bone healing with DBM compared to autologous bone and synthetic bone graft substitutes.<sup>3,38</sup> When DBM was used in a rat craniotomy defect together with a pro-angiogenic compound, both new bone formation and MVD were increased.<sup>39</sup> In a similar manner, hyaluronic acid may serve to stimulate neovascularization when combined with DBM during bone regeneration within ablated marrows of immunocompromised rats.

Effects of NaHY on cells have been previously shown to be dependent on the chain length of the polymer. High molecular weight hyaluronic acid serves as a structural polymer, sequestering growth factors and other signaling molecules.<sup>2,3</sup> In addition, high molecular weight forms of NaHY inhibit endothelial cell proliferation and disrupt endothelial cell monolayers.<sup>14</sup> On the other hand, short, oligomeric fragments of NaHY (less than 20 monomers) have been found to be produced at sites of injury and within

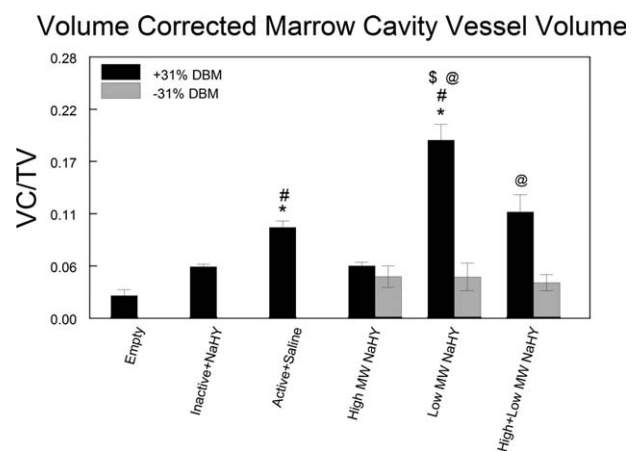


**FIGURE 5.** Corrected total blood vessel volume fraction.  $\mu$ CT total blood vessel volume fractions were adjusted to account for the volume occupied by the DBM within the ablated marrow space. Data are presented as the mean  $\pm$  SEM of nine animals per group. \* $p < 0.05$  versus empty defect; # $p < 0.05$  versus inactive + NaHY; \$ $p < 0.05$  versus active + saline; @ $p < 0.05$  versus no DBM.

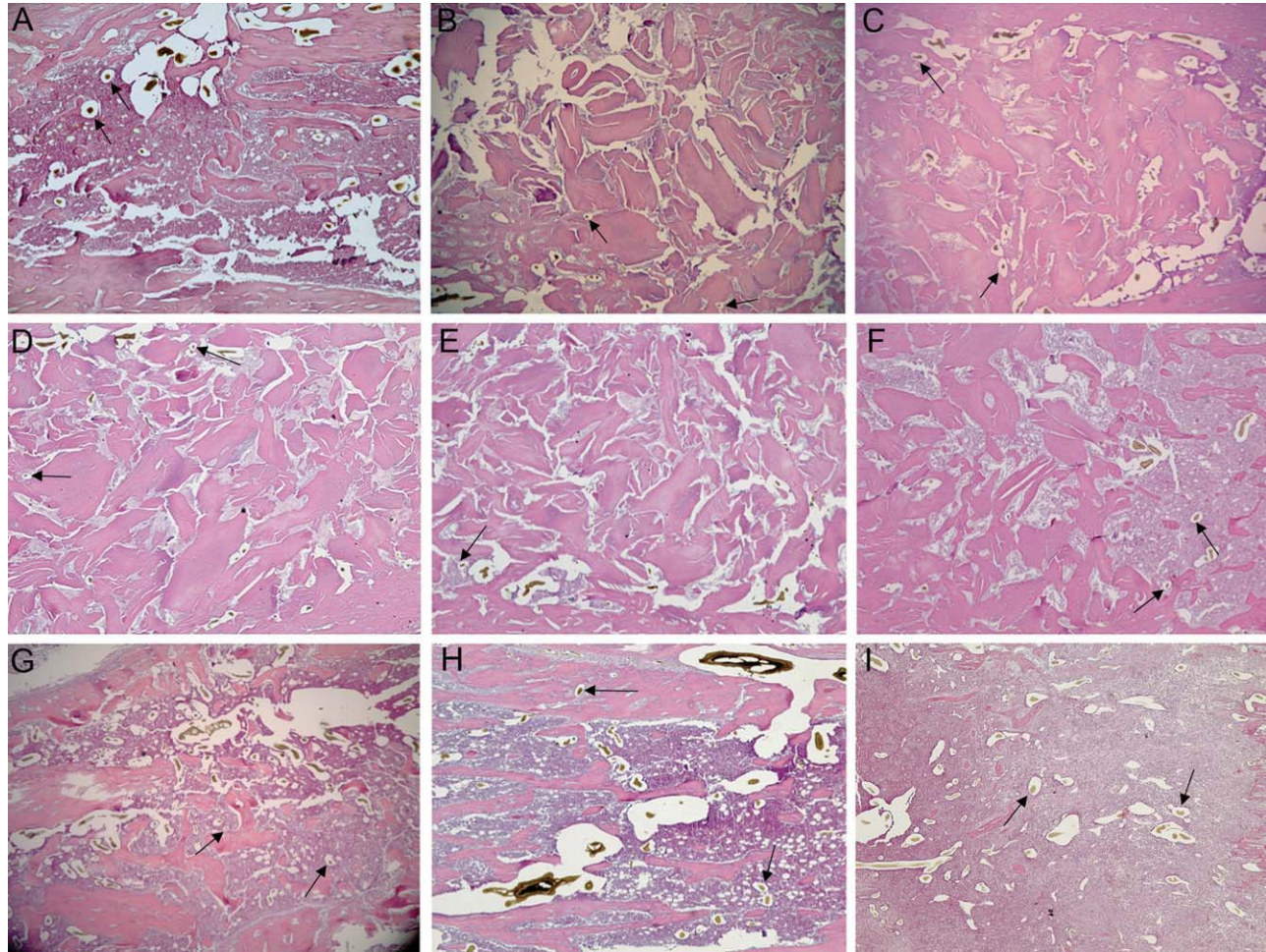


**FIGURE 6.** Representative histological sections of ablated tibias. Following  $\mu$ CT imaging, ablated tibias were embedded in paraffin and processed for histology. Sections were stained with haematoxylin and eosin. Arrows indicate the presence of vascular structures containing Microfil. Groups analyzed were (A) empty defect, (B) Inactive + NaHY, (C) Active + Saline, (D) High MW NaHY + 31% DBM, (E) Low MW NaHY + 31% DBM, (F) High + Low MW NaHY + 31% DBM, (G) High MW NaHY, (H) Low MW NaHY, and (I) High + Low MW NaHY.

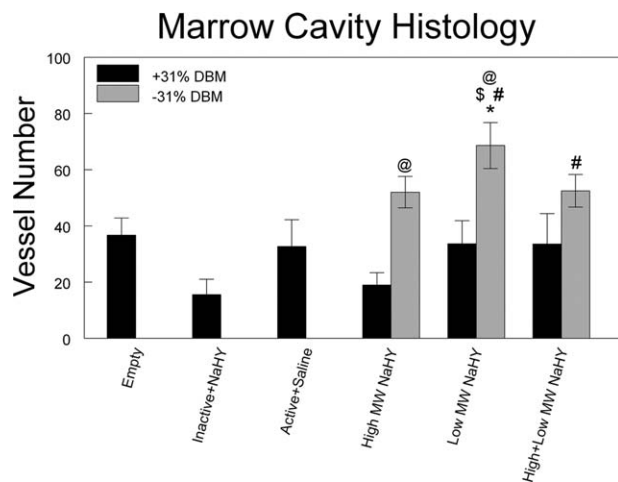


**FIGURE 7.** Effect of tibial marrow ablation on average vessel number within the marrow cavity 14-days post-ablation, determined by histomorphometry. \* $p < 0.05$  versus empty defect; # $p < 0.05$  versus inactive + NaHY; \$ $p < 0.05$  versus active + saline; @ $p < 0.05$  versus no DBM.

tumors.<sup>13</sup> The short NaHY fragments bind to cell-surface hyaluronan receptor proteins such as CD-44, receptor for hyaluronan-mediated motility (RHAMM), and toll-like-receptor-4 (TLR-4).<sup>23</sup> Activation of these receptors on endothelial cells promotes their proliferation and migration, resulting in sprout formation and neovascularization.<sup>40</sup> The ability of NaHY to promote neovascularization has been demonstrated both subcutaneously<sup>41</sup> and in a murine epigastric skin flap model.<sup>42</sup>

High molecular weight hyaluronic acid is broken down *in vivo* by a class of enzymes called hyaluronidases.<sup>43</sup> In particular, hyaluronidase-1 (HYAL-1) is responsible for the generation of short, pro-angiogenic hyaluronic acid oligomers.<sup>18</sup> The generation of these hyaluronic acid oligomers is significantly increased at sites of injury and inflammation.<sup>43,44</sup> While no examination of hyaluronidase expression was performed in this study, it is possible that following injection of NaHY within the ablated marrow, expression of HYAL-1 is increased, resulting in the breakdown of NaHY into smaller fragments, which bind to CD-44 receptors

present on endothelial cells, promoting neovascularization during bone formation.

In our model of tibial marrow ablation, we observed that after 14 days, DBM particulates were still present within the ablated marrow cavities. On the basis of  $\mu$ CT as well as histology observations, we estimated that DBM occupied  $\sim 60\%$  of the total marrow cavity. This results in a decrease in the total volume available for blood vessel invasion. We have demonstrated in this study that the enhanced neovascularization observed in ablated marrows treated with low MW NaHY + DBM is further increased when we account for the volume occupied by the DBM, indicating that the neovascularization induced by NaHY is further stimulated by the presence of DBM.

$\mu$ CT imaging has been shown to be a good model for the three dimensional analysis of vascular structures *in vivo*. The ability of  $\mu$ CT to detect smaller vessels and capillaries is dependent on the resolution of the imaging system and has been investigated previously.<sup>45,46</sup> In the present study, three dimensional reconstructions of the vasculature were generated using a voxel size of 36  $\mu$ m. It is possible in our model of vascular perfusion that the resolution of the  $\mu$ CT imaging system was unable to detect all of the capillaries present in the marrow space, however, a 36- $\mu$ m voxel size has been demonstrated to provide a good analysis of the three dimensional vascular network.<sup>31</sup>

This study was designed to limit the number of animals required to meet the experimental objectives. By using  $\mu$ CT and H&E of decalcified tissues to quantify blood vessel number and volume, all measurements could be made on a single set of animals. For this reason, only static histomorphometry was performed. We did not do dynamic measurements requiring undecalcified sections and fluorochrome labeling. H&E and Microfil were sufficient to identify vascular structures, and for this reason we did not perform immunohistochemistry for endothelial markers like PCAM-1 or von Willebrand's factor. Importantly, the histologic analysis supported the  $\mu$ CT data with regards to blood vessel number.

In conclusion, we have shown here that normal bone healing after tibial marrow ablation is accompanied by an increase in neovascularization within the marrow space, peaking at 14-days post ablation. We also show that NaHY stimulates new blood vessel formation during new bone formation during healing when used as a carrier for DBM. In particular, low molecular weight (35 kDa) NaHY + DBM resulted in increases in total blood vessel volume and total bone volume in ablated limbs. The contribution of the vascularization to remodeling isn't known. In an orthotopic site, low molecular weight NaHY might contribute to bone formation by both supporting MSC and progenitor cell migration in early phases of healing and vascular ingrowth as the NaHY is degraded to smaller fragments. However, as a whole, the data suggest that the increase in neovascularization due to the NaHY may enhance overall bone formation when used as a carrier.

## REFERENCES

1. Degidi M, Artese L, Rubini C, Perrotti V, Iezzi G, Piattelli A. Microvessel density in sinus augmentation procedures using anorganic

- bovine bone and autologous bone: 3 months results. *Implant Dent* 2007;16:317–325.
2. Hallman M, Cederlund A, Lindskog S, Lundgren S, Sennerby L. A clinical histologic study of bovine hydroxyapatite in combination with autogenous bone and fibrin glue for maxillary sinus floor augmentation. Results after 6 to 8 months of healing. *Clin Oral Implants Res* 2001;12:135–143.
3. Abshagen K, Schrodi I, Gerber T, Vollmar B. In vivo analysis of biocompatibility and vascularization of the synthetic bone grafting substitute NanoBone. *J Biomed Mater Res A* 2009;91:557–566.
4. Slevin M, Krupinski J, Gaffney J, Matou S, West D, Delisser H, Savani RC, Kumar S. Hyaluronan-mediated angiogenesis in vascular disease: Uncovering RHAMM and CD44 receptor signaling pathways. *Matrix Biol* 2007;26:58–68.
5. Aslan M, Simsek G, Dayi E. The effect of hyaluronic acid-supplemented bone graft in bone healing: Experimental study in rabbits. *J Biomater Appl* 2006;20:209–220.
6. Jung M, Tuischer JS, Sergi C, Gotterbarm T, Pohl J, Richter W, Simank HG. Local application of a collagen type I/hyaluronate matrix and growth and differentiation factor 5 influences the closure of osteochondral defects in a minipig model by enchondral ossification. *Growth Factors* 2006;24:225–232.
7. Rooney P, Kumar S, Ponting J, Wang M. The role of hyaluronan in tumour neovascularization (review). *Int J Cancer* 1995;60:632–636.
8. Jiang D, Liang J, Noble PW. Hyaluronan in tissue injury and repair. *Annu Rev Cell Dev Biol* 2007;23:435–461.
9. West DC, Kumar S. Tumor-associated hyaluronan: A potential regulator of tumour angiogenesis. *Int J Radiat Biol* 1991;60:55–60.
10. Deed R, Rooney P, Kumar P, Norton JD, Smith J, Freemont AJ, Kumar S. Early-response gene signaling is induced by angiogenic oligosaccharides of hyaluronan in endothelial cells. Inhibition by non-angiogenic, high-molecular-weight hyaluronan. *Int J Cancer* 1997;71:251–256.
11. Slevin M, Krupinski J, Kumar S, Gaffney J. Angiogenic oligosaccharides of hyaluronan induce protein tyrosine kinase activity in endothelial cells and activate a cytoplasmic signal transduction pathway resulting in proliferation. *Lab Invest* 1998;78:987–1003.
12. Slevin M, Kumar S, Gaffney J. Angiogenic oligosaccharides of hyaluronan induce multiple signaling pathways affecting vascular endothelial cell mitogenic and wound healing responses. *J Biol Chem* 2002;277:41046–41059.
13. Slevin M, West D, Kumar P, Rooney P, Kumar S. Hyaluronan, angiogenesis and malignant disease. *Int J Cancer* 2004;109:793–794; author reply 795–796.
14. West DC, Kumar S. The effect of hyaluronate and its oligosaccharides on endothelial cell proliferation and monolayer integrity. *Exp Cell Res* 1989;183:179–196.
15. Sattar A, Rooney P, Kumar S, Pye D, West DC, Scott I, Ledger P. Application of angiogenic oligosaccharides of hyaluronan increases blood vessel numbers in rat skin. *J Invest Dermatol* 1994;103:576–579.
16. Rooney P, Wang M, Kumar P, Kumar S. Angiogenic oligosaccharides of hyaluronan enhance the production of collagens by endothelial cells. *J Cell Sci* 1993;105(Part 1):213–218.
17. Montesano R, Kumar S, Orci L, Pepper MS. Synergistic effect of hyaluronan oligosaccharides and vascular endothelial growth factor on angiogenesis *in vitro*. *Lab Invest* 1996;75:249–262.
18. West DC, Hampson IN, Arnold F, Kumar S. Angiogenesis induced by degradation products of hyaluronic acid. *Science* 1985;228:1324–1326.
19. Acarturk TO, Hollinger JO. Commercially available demineralized bone matrix compositions to regenerate calvarial critical-sized bone defects. *Plast Reconstr Surg* 2006;118:862–873.
20. Kohles SS, Vernino AR, Clagett JA, Yang JC, Severson S, Holt RA. A morphometric evaluation of allograft matrix combinations in the treatment of osseous defects in a baboon model. *Calcif Tissue Int* 2000;67:156–162.
21. Mendes RM, Silva GA, Lima MF, Calliari MV, Almeida AP, Alves JB, Ferreira AJ. Sodium hyaluronate accelerates the healing process in tooth sockets of rats. *Arch Oral Biol* 2008;53:1155–1162.
22. Gao F, Liu Y, He Y, Yang C, Wang Y, Shi X, Wei G. Hyaluronan oligosaccharides promote excisional wound healing through enhanced angiogenesis. *Matrix Biol* 2009;29:107–116.

23. Pardue EL, Ibrahim S, Ramamurthi A. Role of hyaluronan in angiogenesis and its utility to angiogenic tissue engineering. *Organogenesis* 2008;4:203–214.
24. Sasaki T, Watanabe C. Stimulation of osteoinduction in bone wound healing by high-molecular hyaluronic acid. *Bone* 1995;16:9–15.
25. Bab IA. Postablation bone marrow regeneration: An in vivo model to study differential regulation of bone formation and resorption. *Bone* 1995;17(4 Suppl):437S–441S.
26. Kondo N, Tokunaga K, Ito T, Arai K, Amizuka N, Minqi L, Kitahara H, Ito M, Naito M, Shu-Ying J, Oda K, Murai T, Takano R, Ogoose A, Endo N. High dose glucocorticoid hampers bone formation and resorption after bone marrow ablation in rat. *Microsc Res Tech* 2006;69:839–846.
27. Kuroda S, Virdi AS, Dai Y, Shott S, Sumner DR. Patterns and localization of gene expression during intramembranous bone regeneration in the rat femoral marrow ablation model. *Calcif Tissue Int* 2005;77:212–225.
28. Braun G, Kohavi D, Amir D, Luna M, Caloss R, Sela J, Dean DD, Boyan BD, Schwartz Z. Markers of primary mineralization are correlated with bone-bonding ability of titanium or stainless steel in vivo. *Clin Oral Implants Res* 1995;6:1–13.
29. Schwartz Z, Doukarsky-Marx T, Nasatzky E, Goultzschin J, Ranly DM, Greenspan DC, Sela J, Boyan BD. Differential effects of bone graft substitutes on regeneration of bone marrow. *Clin Oral Implants Res* 2008;19:1233–1245.
30. Schwartz Z, Sela J, Ramirez V, Amir D, Boyan BD. Changes in extracellular matrix vesicles during healing of rat tibial bone: A morphometric and biochemical study. *Bone* 1989;10:53–60.
31. Duvall CL, Taylor WR, Weiss D, Guldberg RE. Quantitative micro-computed tomography analysis of collateral vessel development after ischemic injury. *Am J Physiol Heart Circ Physiol* 2004;287:H302–H310.
32. Feldkamp LA, Davis LC, Kress JW. Practical cone-beam algorithm. *J Opt Soc Am A* 1984;1:612–619.
33. Hildebrand T, Laib A, Muller R, Dequeker J, Ruegsegger P. Direct three-dimensional morphometric analysis of human cancellous bone: Microstructural data from spine, femur, iliac crest, and calcaneus. *J Bone Miner Res* 1999;14:1167–1174.
34. Hildebrand T, Ruegsegger P. A new method for the model-independent assessment of thickness in three-dimensional images. *J Microsc* 1997;185:67–75.
35. Kanczler JM, Oreffo RO. Osteogenesis and angiogenesis: The potential for engineering bone. *Eur Cell Mater* 2008;15:100–114.
36. Deckers MM, Karperien M, van der Bent C, Yamashita T, Pappoulos SE, Lowik CW. Expression of vascular endothelial growth factors and their receptors during osteoblast differentiation. *Endocrinology* 2000;141:1667–1674.
37. Carano RA, Filvaroff EH. Angiogenesis and bone repair. *Drug Discov Today* 2003;8:980–989.
38. Boeck-Neto RJ, Artese L, Piattelli A, Shibli JA, Perrotti V, Piccirilli M, Marcantonio E Jr. VEGF and MVD expression in sinus augmentation with autologous bone and several graft materials. *Oral Dis* 2009;15:148–154.
39. Hansen A, Pruss A, Gollnick K, Bochentini B, Denner K, Von Versen R. Demineralized bone matrix-stimulated bone regeneration in rats enhanced by an angiogenic dipeptide derivate. *Cell Tissue Bank* 2001;2:69–75.
40. Cao G, Savani RC, Fehrenbach M, Lyons C, Zhang L, Coukos G, Delisser HM. Involvement of endothelial CD44 during in vivo angiogenesis. *Am J Pathol* 2006;169:325–336.
41. Baier Leach J, Bivens KA, Patrick CW Jr, Schmidt CE. Photocrosslinked hyaluronic acid hydrogels: Natural, biodegradable tissue engineering scaffolds. *Biotechnol Bioeng* 2003;82:578–589.
42. Perng CK, Wang YJ, Tsi CH, Ma H. In vivo angiogenesis effect of porous collagen scaffold with hyaluronic acid oligosaccharides. *J Surg Res* [Epub ahead of print (DOI: 10.1016/j.jss.2009.09.052)].
43. Stern R. Hyaluronan catabolism: A new metabolic pathway. *Eur J Cell Biol* 2004;83:317–325.
44. Noble PW. Hyaluronan and its catabolic products in tissue injury and repair. *Matrix Biol* 2002;21:25–29.
45. Guldberg RE, Ballock RT, Boyan BD, Duvall CL, Lin AS, Nagaraja S, Oest M, Phillips J, Porter BD, Robertson G, Taylor WR. Analyzing bone, blood vessels, and biomaterials with microcomputed tomography. *IEEE Eng Med Biol Mag* 2003;22:77–83.
46. Young S, Kretlow JD, Nguyen C, Bashoura AG, Baggett LS, Jansen JA, Wong M, Mikos AG. Microcomputed tomography characterization of neovascularization in bone tissue engineering applications. *Tissue Eng Part B Rev* 2008;14:295–306.